The Astrophysical Journal, 874:151 (12pp), 2019 April 1 https://doi.org/10.3847/1538-4357/ab07c6

Detection of a Low-frequency Cosmic Radio Transient Using Two LWA Stations

S. S. Varghese[1], K. S. Obenberger[2], J. Dowell[1], and G. B. Taylor[1]
[1] University of New Mexico, Albuquerque, NM, USA; savin@unm.edu
[2] Air Force Research Laboratory, Kirtland AFB, NM, USA
Received 2018 November 7; revised 2019 January 25; accepted 2019 February 16; published 2019 April 2

Abstract

We report the detection of a potential cosmic radio transient source using the two stations of the Long Wavelength Array. The transient was detected on 2017 October 18 08:47 UTC near the celestial equator while reducing 10,240 hr of archival all-sky images from the LWA1 and LWA-SV stations. The detected transient at 34 MHz has a duration of 15–20 s and a flux density of 842 ± 116 Jy at LWA1 and 830 ± 92 Jy at LWA-SV. The transient source has not repeated, and its nature is not well understood. The Pan-STARRS optical telescope has detected a supernova that occurred on the edge of the position error circle of the transient on the same day.

Key words: instrumentation: interferometers – methods: data analysis – radio continuum: general – techniques: image processing

1. Introduction

Radio transient sources can be defined as a class of objects that emit radio waves in the form of bursts, flares, or pulses from short durations (less than a few seconds) to long durations (greater than a few seconds). The progenitors of such sources are usually associated with explosive or dynamic events. Probing such sources helps to understand the physical mechanisms of these extreme energetic events (Cordes et al. 2004). We can classify transients as extragalactic, galactic, and atmospheric based on the location of their occurrence.

Most transients have been discovered through high time resolution (less than a second) observations and blind imaging of the sky. The high time resolution studies at high frequencies have discovered giant pulses from the Crab pulsar at 5.5 and 8.6 GHz (Hankins et al. 2003), single dispersed bursts from rotating radio transients (RRAT; McLaughlin et al. 2006) at 1.4 GHz and the new class of fast radio bursts (FRBs) at 1.4 GHz (Lorimer et al. 2007). Thirteen new FRBs have been detected between 400 and 800 MHz by the Canadian Hydrogen Intensity Mapping Experiment (CHIME) Collaboration (The CHIME/FRB Collaboration 2019a, 2019b). Several high time resolution observation campaigns have been conducted at low frequencies below 300 MHz searching for giant pulses from pulsars, RRATs, and FRBs. At low frequencies, giant pulses from pulsars have been detected, but the detection rate is low for RRATs and zero for FRBs (Coenen et al. 2014; Karako-Argaman et al. 2015; Karastergiou et al. 2015; Eftekhari et al. 2016; Taylor et al. 2016). The scattering of the radio pulses due to inhomogeneities in the medium can cause temporal smearing of the pulse to longer durations at low frequencies. This may limit the detection of short duration transients in the high time resolution observations. This makes fast imaging of the sky on timescales of a few seconds a good option for capturing scatter broadened pulses at low frequencies (Hassall et al. 2013; Trott et al. 2013; Rowlinson et al. 2016).

In the past few decades, blind searches of the sky focused at frequencies above 300 MHz have discovered galactic center transients, bursts from ultra cool dwarfs and flare stars, day scale transients in *Spitzer-Space-Telescope* Wide-area Infrared Extragalactic Survey Deep Field: 1046+59, and 15 transients in the Molonglo Observatory Synthesis Telescope transient survey (Jackson et al. 1989; Hyman et al. 2005; Hallinan et al. 2007; Bannister et al. 2011; Jaeger et al. 2012). The transient radio sky below 300 MHz is not well studied and remains poorly explored below 100 MHz. Fast imaging techniques on shorter timescales are required to capture transient pulses at low frequencies. The initial study of transients were limited by the narrow field of view (FoV) of the radio instruments. With advances in technology, however, new low frequency radio instruments have a wide FoV, increased bandwidth, and sensitivity to study the dynamic transient sky. The currently operating major low frequency radio telescopes include the International Low-Frequency Array (LOFAR; van Haarlem et al. 2013), the Murchinson Wide Field Array (MWA; Tingay et al. 2013), and the Long Wavelength Array (LWA; Taylor et al. 2012; Ellingson et al. 2013).

Several sources have been theorized to emit radio pulses but are yet to be detected. This includes low frequency prompt emission from gamma-ray bursts (Usov & Katz 2000; Sagiv & Waxman 2002), exoplanets (Farrell et al. 1999), giant flares from magnetars or extragalactic pulsars (McLaughlin & Cordes 2003), and annihilating black holes (Rees 1977). Recently, several observing campaigns have been carried out to image the transient sky at low frequencies on integration timescales from 5 s to several hours.

Carbone et al. (2016) conducted a transient search from 115 to 190 MHz using LOFAR with cadences between 15 minutes to several months. No significant transient was found after analyzing 151 images with sensitivity greater than 0.5 Jy obtained from 2275° square survey area.

Stewart et al. (2016) detected a new low frequency radio transient at 60 MHz after 400 hr of monitoring of the North Celestial Pole in the LOFAR Multi Snapshot Sky Survey (MSSS). The identified transient had a flux density of 15–25 Jy with a duration of a few minutes. The transient was not found to repeat after follow-up observations and did not have any obvious optical or high-energy counterparts.

Bell et al. (2014) carried out a transient search on characteristic timescales of 26 minutes and 1 yr with MWA at 154 MHz covering 1430 square degree FoV. The search did not identify any transient sources greater than 5.5 Jy in 51 images obtained from six days of observations.

Rowlinson et al. (2016) searched for transient and variable sources using MWA at 182 MHz. No transients were detected on timescales from 28 s to 1 yr with flux density greater than 0.285 Jy.

Murphy et al. (2017) conducted a transient search on timescales from 1 to 3 yr by comparing the 147.5 MHz TIFR GMRT Sky Survey Alternative Data Release 1 (TGSS ADR1) and the 200 MHz GaLactic and Extragalactic All-sky Murchison Widefield Array (GLEAM) survey catalogs. The search found a transient source with a flux density of 182 ± 26 mJy in the TGSS ADR1 which was not present in the GLEAM survey.

Using the first station of LWA, Obenberger et al. (2014a) detected two kilojansky flux density transient sources while searching for low frequency prompt emission from gamma-ray bursts. These sources were detected at 37.9 and 29.9 MHz with a duration of a few minutes. The transient search was carried out using the all-sky imaging capabilities of the LWA All-Sky Imager (LASI; Obenberger et al. 2015a). Follow-up observations with optical cameras revealed that the radio emission is temporally and spatially associated with optical meteors (Obenberger et al. 2014b). These meteor radio afterglows (MRAs) begin to emit within a few seconds after the optical activity and they can be classified as a new form of atmospheric transient. MRAs were studied extensively to understand the origin and energetics of the emission. The current understanding is that these broadband, nonthermal radio sources are the result of electromagnetic conversion of electrostatic plasma waves within the turbulent plasma of meteor trails (Obenberger et al. 2015b).

With a detection rate of 60 MRAs per year, it is difficult to differentiate these foreground sources with events of cosmic origin using a single LWA station. The earlier transient studies using a single LWA station (Obenberger et al. 2014a, 2014b) assumed that all unpolarized transients lasting from a few seconds to a few minutes in duration were MRAs. However, some of the events assumed to be MRAs might have been cosmic in nature, but there was no way to properly identify the transients not directly associated with an optical meteor. The recent commissioning of the new LWA station at Sevilleta National Wildlife Refuge (LWA-SV) provides a new opportunity to observe cosmic transients. The two stations are separated by 75 km, which is sufficient to differentiate the foreground transient events like lightning, MRAs, radio frequency interference (RFI), and low earth orbit satellites from cosmic events, while still being close enough to share over 99% of the sky. So far LOFAR MSSS is the only low frequency survey that has carried out the transient search close to the LASI operating frequency with wide FoV.

In this paper, we present a 2 yr study of all-sky images from both LWA stations that has identified a new promising cosmic transient candidate. Sections 2 and 3 describe the observations and data reduction methodology. Section 4 describes the detection of the cosmic transient candidate event. Section 5 gives an extensive analysis of the common transient events observed in both LWA stations and explains why one transient event is a statistically significant and promising candidate.

2. Observation

The first station of the Long Wavelength Array (LWA1) is a low frequency radio telescope located in central New Mexico (Taylor et al. 2012). The telescope operates between a 10 and 88 MHz frequency range and it is collocated with the Karl G. Jansky Very Large Array (VLA). The array is comprised of 256 dual polarization dipole antennas along with five additional outrigger antennas located at 200–500 m distance from the center of the array. The core of the array is distributed in the form of a 100 × 110 m ellipse.

The second station, LWA Sevilleta (LWA-SV), was commissioned in 2017 November (Cranmer et al. 2017). LWA-SV is located at the Sevilleta National Wildlife Refuge, 75 km northeast of LWA1. LWA-SV has a similar layout to LWA1 and the backend hardware has similar but not identical capabilities.

Both the stations primarily operate in two modes, digital beamforming and the all-sky mode. In the digital beamforming mode, a time domain delay-and-sum architecture is used to form beams. The delay processed signals from each antenna can be added to form up to four independently steerable dual polarization beams at any direction in the sky. Each beam can be tuned to two central frequencies within the operating range of the telescope with a bandwidth up to 19.6 MHz in LWA1 and 9.8 MHz in LWA-SV.

The all-sky mode takes advantage of the primary beam of a single dipole antenna, which is sensitive to the whole sky. The all-sky monitoring is done in Transient Buffer Wide (TBW) and Transient Buffer Narrow (TBN) modes. In the TBW mode, the voltage time series from each antenna is collected at the entire 78 MHz bandwidth for 61 ms and it takes 5 minutes to write out the data. TBN mode collects the voltage series time series data from each antenna continuously at 100 kHz bandwidth and can be tuned to anywhere in the operating frequency of the stations. The collected data is then sent to a software FX correlator (Ellingson et al. 2013).

LASI is the back end correlator for both LWA stations (Obenberger et al. 2015a). LASI cross-correlates real time TBN data from each antenna and produces an all-sky image every 5 s. The produced images are uploaded to the LWA TV website[3] and stored in the LWA archive.[4] For this work, we have used over 10,240 hr (2016 May–2018 July) of data recorded from each LWA station at 34 MHz and at 38 MHz.

3. Data Reduction

3.1. Transient Pipeline

The transient search pipeline uses an image subtraction algorithm to find the transient candidate events from both stations (Obenberger et al. 2015a). In the image subtraction process, an average of the previous six images is subtracted from the running image. At the same time the script masks out the bright radio sources like Cyg A and Cas A for efficiently finding transients. The pixels with flux density greater than 6σ in the subtracted image are marked as transient candidates. The detection threshold varies near the Galactic plane and has been discussed in Obenberger et al. (2015a). Currently the transient search is carried out on 5, 15, and 60 s integrations in Stokes I and V.

3.2. Comparison of Transient Events

The pipeline outputs the time and coordinates of the transient events detected from each LWA station. The noise of the LWA1 subtracted image measured at 38 MHz is 41 Jy at zenith

[3] http://www.phys.unm.edu/~lwa/lwatv.html
[4] https://lda10g.alliance.unm.edu/

and increases toward the horizon (Obenberger et al. 2015a). The LWA-SV station is 5%–10% more sensitive than the LWA1 station because it has more fully functioning dipoles. Depending on the location of a transient event occurring from the zenith of each station, image noise changes and leads to some time difference in detecting them at each station. We compare the output files from both stations to find the associated events that occur within 30 s difference.

The next step is to look for cosmic transient candidates and meteor afterglow candidates. If the angular difference between coordinates of events detected from each station is less than 3°, then it is classified as a cosmic transient candidate. Since cosmic transient events occur at great distances compared to the 75 km baseline, the angular direction to the event from each station would be the same. If the angular difference is greater than 3°, then it is classified as an MRA candidate. The 3° angular difference threshold is given in order to account for the pointing of telescope and random errors from ionospheric disturbances. For a 75 km baseline, 3° angular difference corresponds to a distance of 1400 km.

The main advantage of this method is to detect common events that can be cosmic or meteor afterglow candidates. Also at the same time it removes nearly all the local RFI effects arising from power lines, lightning, air planes, etc. However, it still identifies some false positive events like scintillation and radio transmitter signal reflections from meteor trails.

The whole process of finding transients using the two stations is automated. Once LASI collects the all-sky images for a day, the transient search pipeline processes all the data and finds the transient candidates. At the end of each UT day, the collected events from each station are compared, and events that are classified as either an MRA or a cosmic transient are emailed to the authors of this study.

4. Cosmic Transient Candidate Detection

The radio transient candidate LWAT 171018 was detected after analyzing the archival all-sky images from the two LWA stations. The events took place on 2017 October 18 (MJD 58044) 8:47:33 UTC in LWA-SV and 8:47:38 in LWA1. The LASI correlator was collecting the all-sky images at 34 MHz in both stations. Each station recorded the event in the adjacent time bins where each bin is a 5 s integration. The event detection in each station can be considered to be simultaneous within the uncertainty of our measurement. The top panel in Figure 1 shows the Stokes *I* light curves of the transient event seen from each station.

There is difference in the signal to noise in both stations due to the difference in the number of working antennas. The light curves show that the emission lasted for 15–20 s in each station. LWA1 has recorded 7.24σ source signal and LWA-SV has 8.81σ detection from the all-sky image indicating that the emission is relatively faint. The bottom panel in Figure 1 shows the subtracted image of the transient seen from LWA1 and LWA-SV, which suggests that it is a point source. There is more noise in the LWA1 image compared to LWA-SV. The different ionosphere above each station and the noise being added during averaging in the image subtraction may lead to small difference in apparent source structure, which is evident from the images.

The all-sky image from the time of peak emission was used to accurately measure the flux density. The average of 10 noise-like images is subtracted from the peak flux image to measure the peak flux density of transient and thermal noise in arbitrary units. The thermal noise is calculated by the standard deviation from a quiet portion of the subtracted image. The flux and noise values were calibrated using the bright radio source Cyg A, scaling them to jansky. The measured value of transient flux density from the LWA1 is 842 $\pm$ 116 Jy and at LWA-SV is 830 $\pm$ 92 Jy. The calculated error bars are thermal noise values from the peak flux image.

5. How to Confirm the Transient

The presence of similar light-curve patterns and close flux density values is not sufficient evidence by itself to confirm a cosmic origin. In the automated transient search pipeline, the comparison script looks for power spikes happening in both stations that are within a 5 s interval. The power spike at the same time in both stations could have a number of origins. Below we examine each of the possible origins.

MRAs—The MRA events usually occur at 90–130 km elevation. The difference in angular direction to the event from each station can vary from 30° to 45° in the sky as the two stations are separated by 75 km. Therefore the two station will not record MRAs in the same angular directions (R.A., decl.) and they can be ruled out.

RFI—These are mostly man-made signals reflecting off the ionosphere and meteor plasma trails. The origin of RFI seen in both stations can be from the same or different transmitters. The reflection events are typically bright, short in duration, highly linearly or circularly polarized, and are narrowband in frequency. Figure 2 shows the light curves of the event at stokes *Q, U*, and *V* from both stations. The all-sky image data is collected at 100 kHz bandwidth and the spectrum information is not available as the measurement sets are deleted after one month from the day of observation. This limits looking into the raw data for narrowband RFI events. But the lack of a polarized detection in both stations suggests that we can rule out the case of coincident RFI.

Scintillation—Scintillation of bright radio sources by Earth's ionosphere is a problem at lower frequencies (Obenberger et al. 2015a). The ionosphere contains magnetized plasma and density variations, which cause rapid changes in observed flux (up to a factor of 15) and can offset the position of sources by a few degrees. This effect becomes intense for bright compact sources and at the same time sources below the nominal detectable limit can appear above the noise floor for some period of time. The scintillation seen in each station can be due to the same or different radio sources. In order to reduce false transient events due to scintillation, the script masks radio sources brighter than 50 Jy from the VLA Low Frequency Sky Survey at 74 MHz (VLSS; Cohen et al. 2007; Lane et al. 2012). This removes a significant portion of the sky ($\approx$12%) but is the best way to avoid confusion between transients and scintillation.

A full statistical analysis determining the rates of scintillation based on sky position, flux density, and source structure are beyond the scope of this paper. However, anecdotal evidence suggests that sources as low as 10 Jy (at 74 MHz) can scintillate to detectable levels. It is therefore helpful to calculate the probability that a random transient will be spatially coincident with a VLSS source with flux density greater than 10 Jy at the same LST of LWAT 171018 detection. Using a Monte Carlo simulation with 10^5 beams and the VLSS catalog, we estimate

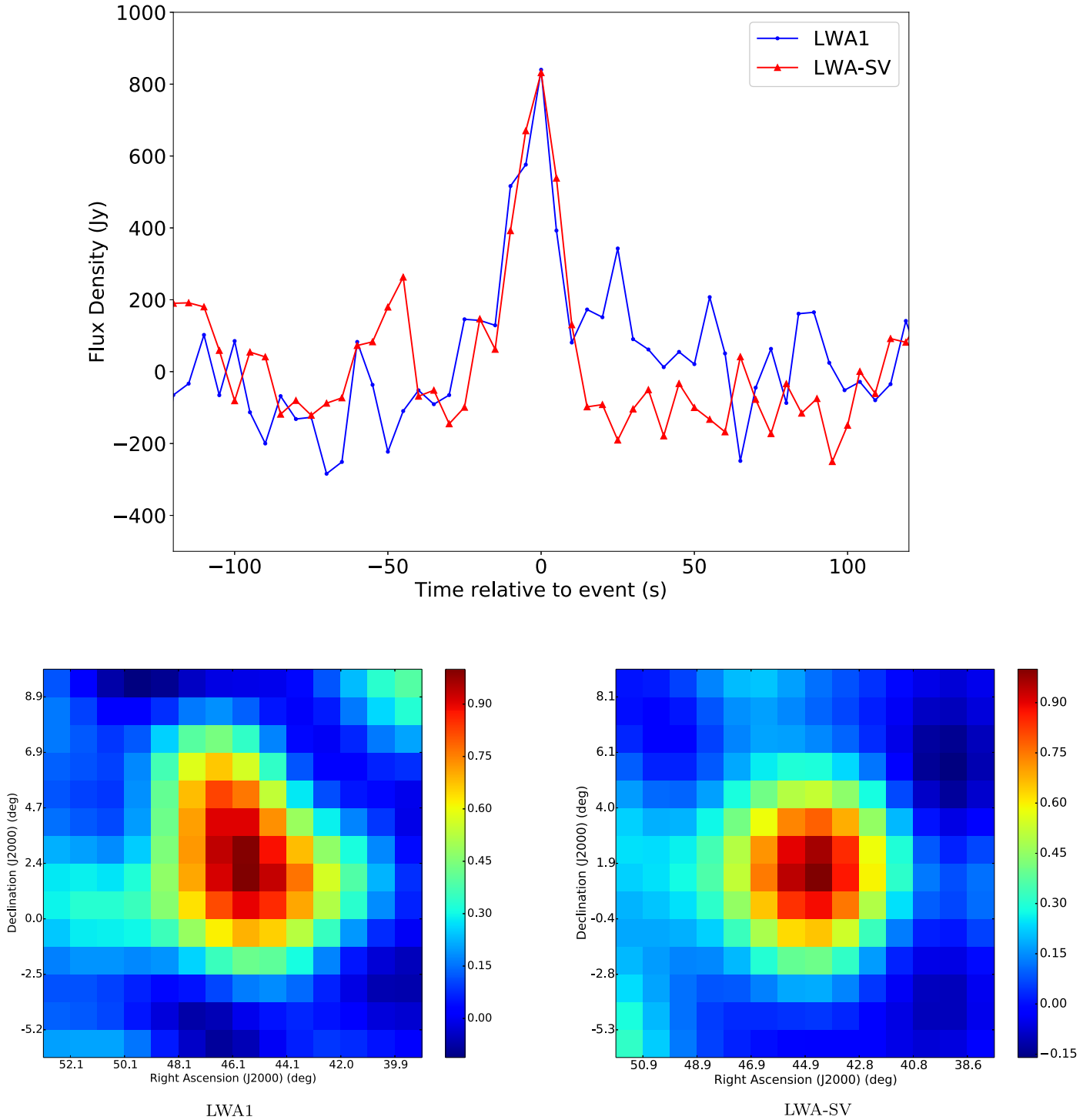

Figure 1. Stokes *I* light curves of the transient event LWAT 171018. The blue light curve denotes LWA1 and the red curve denotes LWA-SV. The bottom panel shows the subtracted image of the transient from each station. The color bar shows the normalized pixel values in the subtracted image. Each pixel in the image corresponds to $1.^{\circ}016$ on the sky.

a 15% chance that a VLSS source >10 Jy will be within the position error of a random transient.

Typical scintillation light curves are characterized by random fluctuations with several peaks appearing over a period of about 30 minutes to a few hours. The transient search algorithm may identify these peaks as transients. While scintillating sources often trigger a single station transient, a single source typically does not experience a scintillation spike at both stations at the same time. However, during periods with exceptionally high scintillation, double station triggers can occur; these triggers then show up as potential cosmic transients. In the data presented in this paper, we have observed 18 cases of double station coincident source scintillation. Such cases are easy to identify due to their characteristic light curves, and the fact that they typically occur during periods of high scintillation, where many other sources are scintillating at the same time. We have also identified one case of a coincident RFI event in both stations.

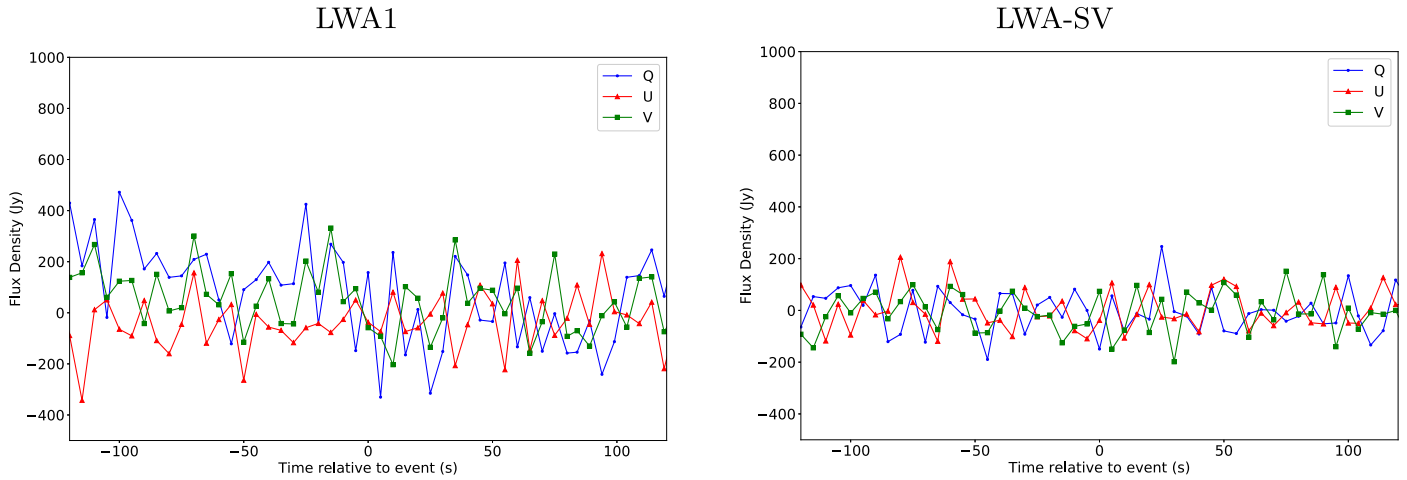

Figure 2. Stokes *Q, U*, and *V* light curve of the transient event from LWA1 (left) and LWA-SV (right).

A statistical approach was required to study the nature of scintillation events and to differentiate them from real cosmic transient events. For this study, we chose two cases based on their occurrence at the same time and high flux density levels. The first case is our promising, transient event LWAT 171018. The second case is the scintillation candidate MJD 58040. The details of all the scintillation and RFI events are given in Table 1. The nature of the unknown event in LWA1 from MJD 58238 is not clear. This could be an MRA event seen by LWA1 that was not in the shared sky region of LWA-SV.

Four methods are used here to analyze the scintillation candidate MJD 58040 and LWAT 171018 to understand their significance.

The first method is to look at the light curves of the events from each station as well as the averaged light curves. For a light curve with a Gaussian noise, averaging of the light curves from both stations will increase the signal-to-noise ratio (S/N) for a real signal.

Figure 3 shows the light curves from each station and their average for LWAT 171018. In the light curves, the event is defined as the time from 10 s before and after the peak flux point, which is denoted as zero seconds. Noise is defined as all the points in light curve other than the event. The light curves from each station has Gaussian noise and similar peak flux density at the same time. The S/N has increased significantly in the averaged plot curves. Figure 4 shows the light curves from the scintillation candidate MJD 58040. In the light curve plots, the noise is fluctuating with random peaks over the course of more than an hour. Adding the light curves from both stations has increased the S/N for the scintillation candidate MJD 58040. Even though the S/N has increased, the light curves still have random fluctuations as high as the peak signal.

Figure 5 shows the scattered plot of the transient flux density for LWAT 171018 and scintillation candidate MJD 58040 from each station. The plots give a good estimate of the statistical significance based on the distribution of noise and peak flux for each case. For LWAT 171018, the noise distribution is clustered and the transient event is well separated from noise suggesting that it is significant. But for scintillation candidate MJD 58040, the noise has a scattered distribution and the transient event is immersed in the noise.

Figure 6 shows the histogram plots made from the light curves of LWAT 171018 and scintillation candidate MJD 58040 respectively. The histograms fitted with a Gaussian

Table 1
List of Cosmic Transient Candidate Events Detected from Both LWA Stations and Their Classification

MJD (1)	UTC Time (2)	LWA1 (3)	LWA-SV (4)	Kurtosis LWA1 (5)	Kurtosis LWA-SV (6)
58019	01:42	RFI	RFI	1.153	37.438
58039	05:43	Scintillation	Scintillation	0.719	4.324
58040	05:26	Scintillation candidate	Scintillation candidate	2.067	4.817
58044	08:47	LWAT 171018	LWAT 171018	0.056	0.161
58054	05:36	Scintillation	Scintillation	1.447	5.386
58064	15:28	Scintillation	Scintillation	132.226	17.766
58066	04:30	Scintillation	Scintillation	5.133	1.834
58067	12:33	Scintillation	Scintillation	−0.0445	1.612
58094	08:06	Scintillation	Scintillation	0.664	2.201
58102	05:32	Scintillation	Scintillation	2.537	73.111
58102	11:15	Scintillation	Scintillation	2.534	27.901
58113	06:42	Scintillation	Scintillation	0.639	5.354
58128	09:35	Scintillation	Scintillation	1.033	1.966
58174	08:31	Scintillation	Scintillation	4.282	1.191
58238	02:58	Unknown	Scintillation	0.538	73.279
58238	04:57	Scintillation	Scintillation	2.167	6.674
58238	05:01	Scintillation	Scintillation	4.779	3.721
58341	10:25	Scintillation	Scintillation	0.672	2.177
58356	17:14	Scintillation	Scintillation	0.675	1.449

profile provide a better picture to understand the distribution of noise and the transient event. The noise is more or less Gaussian in both histograms. The LWAT 171018 is well separated from noise where it is not in scintillation candidate MJD 58040 as the tail of the Gaussian fit goes to higher flux density values.

The analysis of two events based on the light-curve pattern, scatter plots, histograms, and S/N suggest that the LWAT 171018 is significant and different from the scintillation candidate MJD 58040. Furthermore, it also demonstrates that the LWAT 171018 observed by two stations is not a coincident random spurious signal but a real one.

In order to characterize the scintillation better, an index or a statistical parameter was necessary. The kurtosis of a probability distribution can be used as an index for measuring the amount of scintillation. In probability and statistics, kurtosis

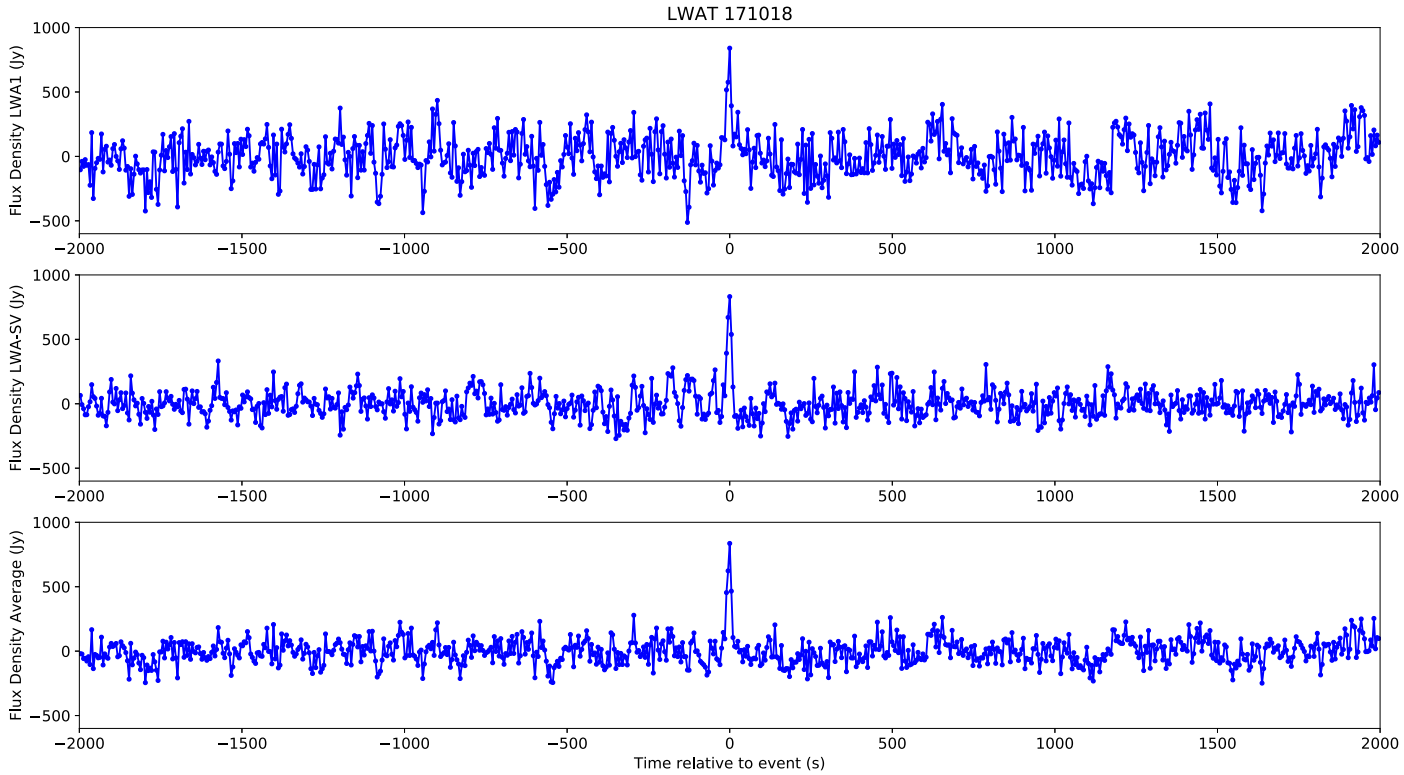

Figure 3. Plot showing the light curves of LWAT 171018 on a longer time axis. The first top panel shows the light curve of the event from LWA1 with S/N = 5.28. The middle panel shows the light curve from LWA-SV with S/N = 8.44. The bottom panel shows the average light curve from both stations with an improved S/N = 9.18. The time zero denotes the peak time of the event.

is defined as the ratio of fourth central moment and square of variance. In simple words, kurtosis gives the measure of the infrequent outliers in a distribution. The kurtosis value for a Gaussian distribution in Fisher's definition is zero. Kurtosis of the light curve in each station before and after the event can be calculated to understand how deviant the noise is from a Gaussian distribution. If we use the kurtosis as a measure of scintillation, low kurtosis or close to zero kurtosis events should be scintillation quiet and high kurtosis events should be high scintillation. This exercise was carried out for all the 19 commonly detected events, one hour before and after the peak event and the values are listed in Table 1. Figure 7 shows the plot of measured kurtosis value for each event in both stations. The LWAT 171018 has a kurtosis value close to zero in both stations whereas all the other events have much higher kurtosis values. There are some scintillation events with high kurtosis value in one station and low kurtosis value in the other station. The high kurtosis value in one station is basically due to the presence of bright, short duration RFI spikes along with the source scintillation. The close to zero kurtosis values in both stations suggests that LWAT 171018 is different from other events and the origin of such a signal is not due to scintillation.

While the source appears statistically separate from scintillating sources, there is a 25 Jy (at 74 MHz) source, 4C +1.06, within error circle plot (see Figure 9). 4C +1.06 appears to be a 30 arcsec compact radio source from the 20 cm VLA observations (Roland 1985). The scintillation of this source has triggered the single station transient pipeline numerous times in the two years of data used in this study. The source has shown up on 15 occasions in LWA-SV and 9 different occasions in LWA1, but LWAT 171018 is the only time a source has shown up in both statons at the same time. Despite the fact that LWAT 171018 appears different from these scintillation events, it remains a possibility that the two coincident events were two, unlucky scintillation spikes from 4C +1.06. We note however, that as mentioned above there is a 15% chance that a random event will be spatially coincident with a VLSS source bright enough to be detected through a scintillation spike. So the fact that LWAT 171018 is spatially coincident with 4C +1.06 could simply be an unlucky coincidence.

In order to understand more about the scintillation of 4C +1.06 triggered in each station, the kurtosis one hour before and after the event as well as the peak fluxes were calculated. The 4C +1.06 source was observed to scintillate with an average peak flux of 6.20σ and a kurtosis of 0.66 in LWA1 and with an average peak flux of 6.01σ and a kurtosis of 3.12 in LWA-SV. Figure 8 shows the histogram of the kurtosis measured during the scintillation of 4C +1.06 that occurred on different occasions in each station. The source has experienced low and high scintillation in both stations at different times. But none of the events were measured with a close to zero kurtosis value, which was observed for LWAT 171018. This suggests that LWAT 171018 is less likely a coincident scintillation spike from 4C +1.06.

Satellites—The next possible candidate is the reflection or unknown emission from satellites. The low Earth orbit satellites can be ruled out as their spatial position changes in the all—sky images. Our transient case is a stationary point source suggesting the possibility of geostationary satellites. Various websites are available on the internet for tracking the position of satellites. By tracking the position of satellites above the horizon of both stations using the In-The-Sky.org website,[5] one

[5] https://in-the-sky.org/satmap_worldmap.php#

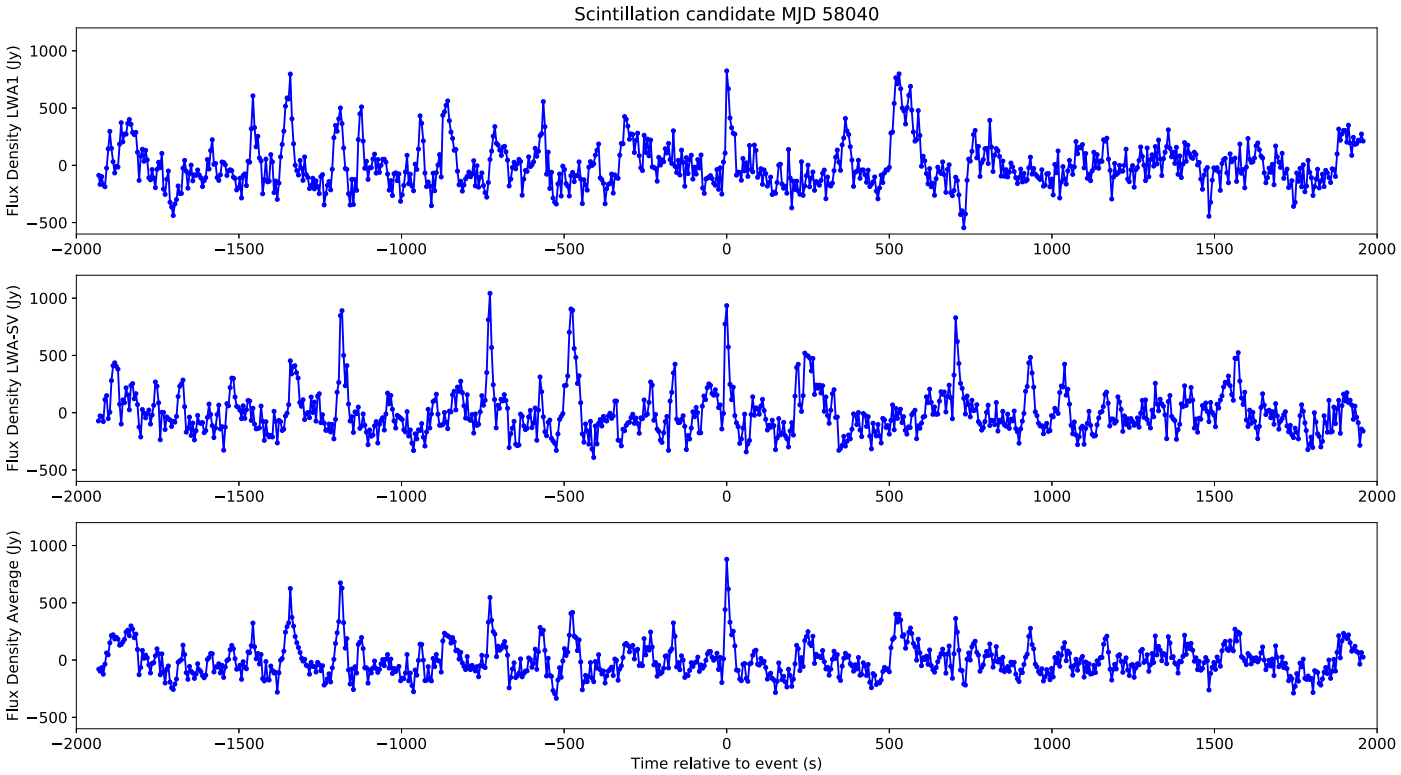

Figure 4. Plot showing the light curves of the scintillation candidate MJD 58040 on a longer time axis. The first top panel shows the light curve of the event from LWA1 with S/N = 4.25. The middle panel shows the light curve from LWA-SV with S/N = 4.88. The bottom panel shows the average light curve from both stations with an S/N = 6.42. The time zero denotes the peak time of the event

candidate satellite was found in the vicinity of the transient. The satellite was Morelos 3, a Mexican communication satellite that is designated to transmit at 1–2 GHz and 12–18 GHz.

Reflections from a satellite requires dimensions on the order of wavelengths. At 34 MHz ($\lambda = 9$ m), the longest dimension of the fully expanded configuration of the satellite[6] is 41 m (4.5λ). While an object of this size is capable of scattering a 34 MHz wave, it is so small that a bright reflection is unlikely. Moreover, the reflection of man-made RFI (the only thing possibly bright enough) would be strongly polarized, which is not the case for the transient reported here.

Alternatively, since transmitters are imperfect, there could be a possible unpolarized out of band emission from satellite transmitters at lower frequencies. As of now, we do not know the origin of any such emission mechanisms. The Morelos 3 was launched in 2015 October and both LWA stations have been collecting all-sky images since 2016 May. If this was a signal from the satellite, one or both stations would likely see the signal at other times. In order to check for any kind of previous signals from geostationary satellite, the all-sky image from both stations were searched at the corresponding azimuth and altitude locations. We could not find a single case of emission at the position of the satellite.

Figure 9 shows the 1σ position error circle plot from each station along with the location of transients, satellites, VLSS sources 4C +1.06, NGC 1218, 4C +04.11, and an optical supernova detected in the vicinity. The position error for each telescope takes into account the pointing error of the telescope, signal-to-noise error, and the random error due to ionospheric fluctuation at low frequencies. This estimated value of position error was $1^{\circ}.19$ for LWA1 and $1^{\circ}.15$ for LWA-SV.

6. Discussion

6.1. Optical or High-energy Counterparts

Having ruled out all the known cases of false positive events, we are left with a previously undiscovered cosmic signal. We searched for any optical or high-energy counterparts, including gamma-ray bursts, flare stars, bright radio sources, and standard supernovae. We noticed that a standard supernova went off in the same direction (03:04:39.35, +03:21:32.52) of the sky on the same day at 11:38:24 UTC. The optical supernova, AT 2017hps was detected by the Pan-STARRS1 group (Transient Name Server[7]; The Open Supernova Catalog[8]; Guillochon et al. 2017) and the location of the transient is marked on the position error plot (see Figure 9). A standard supernova occurs frequently in all directions of the sky and the possibility of low frequency radio emission from them is not clear. Forty-six supernovae were detected within ±2 days of the event in different parts of the sky with a decl. greater than -25°.

An estimate of the probability can be calculated by assuming that all the supernovae events occurred randomly in the sky 30° above the horizon. For this purpose, the radius of the error circle is the position error in LWA1, which is $1^{\circ}.19$ (1/48 rad).

$$\text{Probability} = \left[\frac{\text{Number of supernovae events}}{\text{Number of beams (error circles)}}\right]. \quad (1)$$

[6] http://spaceflight101.com/atlas-v-morelos-3/morelos-3/

[7] https://wis-tns.weizmann.ac.il/object/2017hps/discovery-cert

[8] https://sne.space/

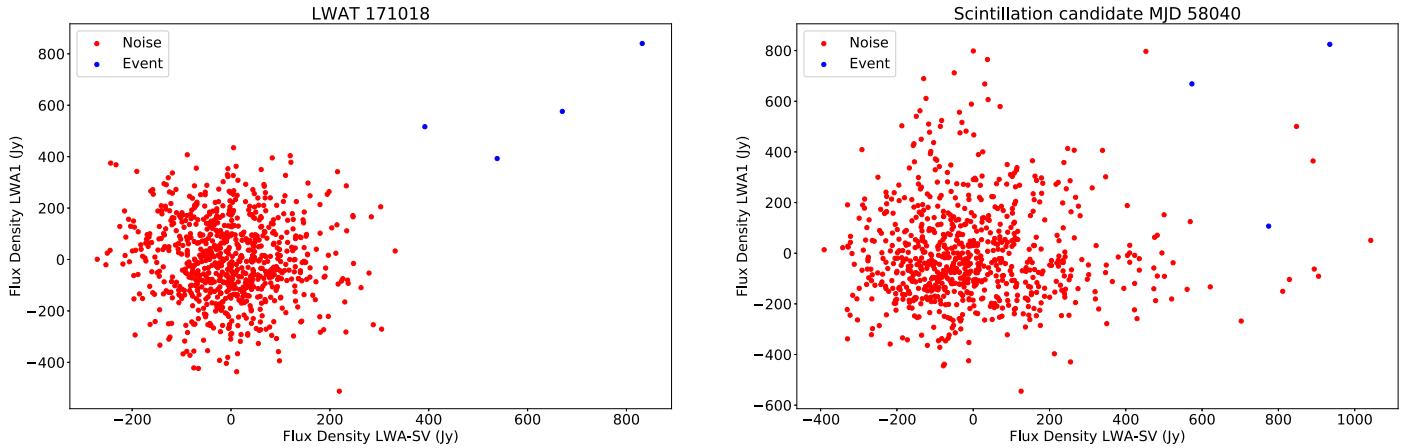

Figure 5. Scattered plot of the flux density from both stations of LWAT 171018 (left) and scintillation candidate MJD 58040 (right). The event is defined as the time from 10 s before and after the peak flux point, which is denoted as zero seconds in the light curve. Noise is defined as all the points in the light curve other than the event. The red points denote the noise and blue points indicate the transient event.

$$\text{Number of beams} = \left[\frac{\text{Area of LWA sky}}{\text{Area of beam}}\right]. \quad (2)$$

$$= \frac{\pi \text{ rad}^2}{\pi\left(\frac{1}{48} \text{ rad}\right)^2} = 2304. \quad (3)$$

$$\text{Probability} = \frac{46}{2304} = 1.98\%. \quad (4)$$

So the probability of a standard supernova to occur within the positional error circle of both LWA stations is 1.98%.

6.2. New Radio Transient

The lack of evidence supporting the false positive detections and the absence of any clear optical or high-energy counterpart suggests that this could possibly be a new type of cosmic event. Previous observations have not detected any such kind of high flux density transient events at low radio frequencies. We have only detected this one event since LASI began producing all-sky images from both stations in 2016 May. With respect to the data used for this study, the new transient source does not repeat. The nature of the transient is not clear as it lacks other EM counterparts and has only occurred once.

The single cosmic transient event was detected after 10,240 hr of observation. Each hour has 720 all-sky images and each image has 2304 independent beams in the sky 30° above the horizon. This makes a total of 1.70×10^{10} independent beams. For Gaussian statistics, the probability of finding a 5.28σ detection in LWA1 is 6.46×10^{-8} and 8.46σ in LWA-SV is 1.34×10^{-17}. The joint probability of finding such an event simultaneously in both stations is given by their product, which is 8.64×10^{-25}. The expected number of such events we should have seen is given by the product of the joint probability and number of independent beams. For the 1.70×10^{10} independent beam integrations observed with both stations the calculated number of such events is $\approx 1.47 \times 10^{-14}$. This is much less than one implying that this is a real event and not just a chance occurrence of two simultaneous noise peaks.

The radio waves traveling through the ionized plasma in the intergalactic medium cause a difference in the arrival time of signals. Higher frequency signals will arrive first and the measured pulse over a frequency bandwidth will be dispersed. An upper limit of the dispersion measure (integrated electron density along the line of sight) can be calculated using the pulse width of the transient from the light curve. The dispersion measure is calculated on the assumption that the pulse is dispersed along 100 kHz bandwidth of the TBN data. The relation between time delay in the arrival of two different frequencies and dispersion measure is given by

$$\Delta t_d = 4.149 \times 10^3 \frac{\text{MHz}^2 \text{ cm}^3 \text{ s}}{\text{pc}} \left(\frac{1}{f_1^2} - \frac{1}{f_2^2}\right) \text{DM}. \quad (5)$$

In the above equation, DM is the dispersion measure, Δt_d was taken to be 15 s from the light curve, $f_1 = 33.95$ MHz and $f_2 = 34.0375$ MHz. Putting all these values in Equation (5) will return a DM = 804 pc cm^{-3}. If we compare the DM value with the known transient sources, it will fall into the group of recently detected FRB events. Lorimer et al. (2007) detected the first FRB in 2007 at 1.4 GHz after analyzing the archival survey data of Magellanic clouds using Parkes Radio telescope in Australia. The burst had a flux density of 30 Jy and a duration of 5 ms. The pulse was dispersed with a DM of 375 pc cm^{-3} and was far away from the Galactic plane suggesting an extragalactic origin. In later years, further observations using Parkes, GBT, Arecibo have discovered over 17 FRBs at high frequencies and these are listed in the FRB catalog (Petroff et al. 2016). Recently, the CHIME/FRB Project discovered 13 new FRBs at frequencies between 400 and 800 MHz in their precommissioning phase. One of the detected FRBs was observed to have six repeated bursts. The hypothesized origin of these short bursts was thought to be exotic phenomena like merging neutron stars or evaporating black holes. The detection of repeating bursts eliminates the cataclysmic models for the FRB source (The CHIME/FRB Collaboration 2019a, 2019b). However, no FRBs have been detected below 100 MHz.

An FRB is potentially a good candidate for LWAT 171018. Pulse broadening can occur at lower frequencies due to dispersion and scattering causing seconds of time delay. Since the calculated upper limit of DM is high and the source location is far away from the Galactic plane ($l = 176.13$, $b = -46.88$), the transient could be possibly an extragalactic source.

The expected scattering width at 34 MHz can be calculated using the relation

$$\tau_{sc}(\nu) \propto \nu^{\gamma}, \quad (6)$$

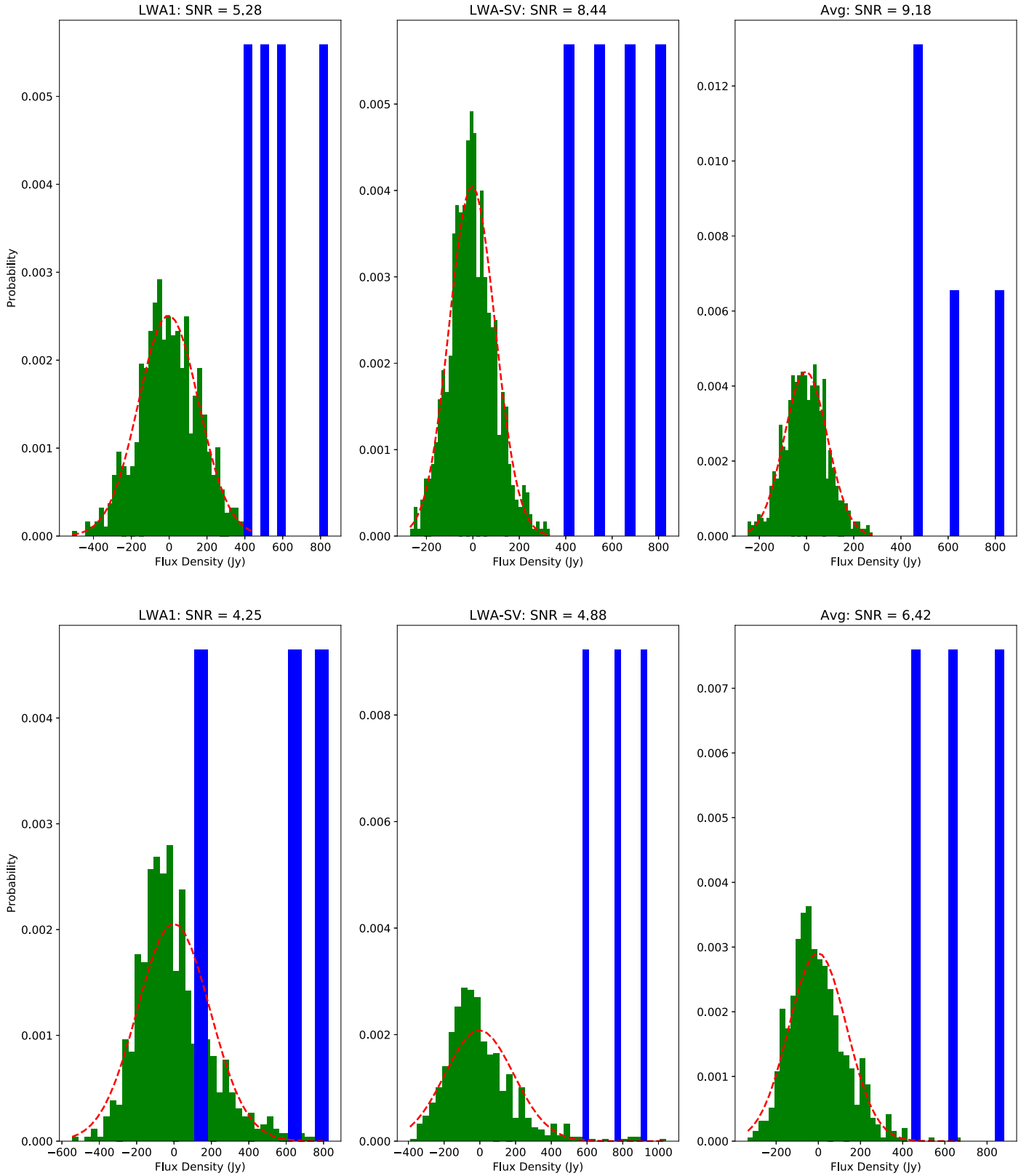

Figure 6. Histogram plot of the transient event LWAT 171018 (top) and scintillation candidate MJD 58040 (bottom) from the light curves of LWA1, LWA-SV, and their average. The green bars show the noise that is fitted with a Gaussian distribution. The blue bars denote the transient event. The calculated S/N is shown in the title of each histogram

where τ_{sc} is the scattering timescale and γ is the scattering index which is taken to be -4 for this case. For a short duration, <1.1 ms FRB pulse from Thornton et al. (2013) at 1.3 GHz, the estimated pulse width at 34 MHz is ≈2400 s. The measured 15 s pulse width from light curve is much less than the expected pulse width due to scatter broadening.

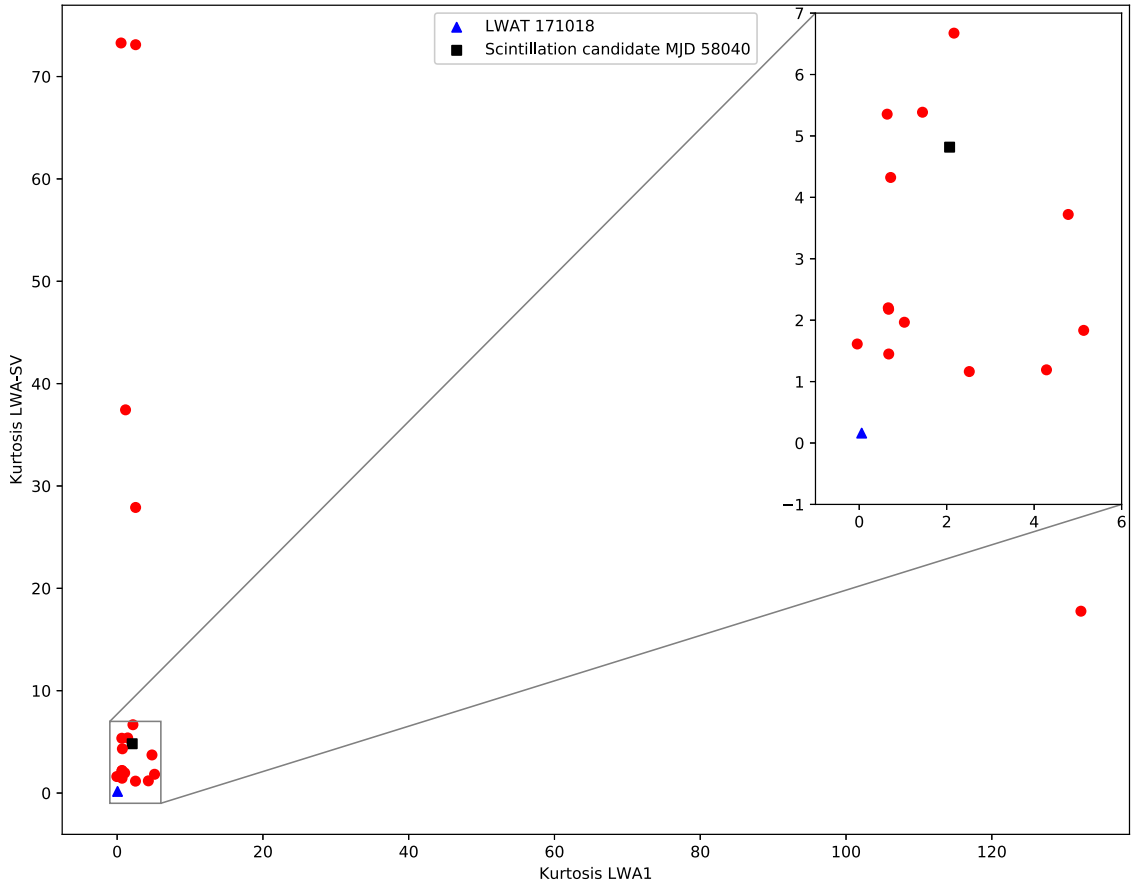

Figure 7. Kurtosis plot of the light curves from LWA1 and LWA-SV for each common event listed in Table 1. The rectangle shows the zoomed portion of the closely associated points toward origin.

Several other imaging campaigns have been conducted at low frequencies for FRB detection. Tingay et al. (2015) searched for FRBs using MWA between 139 and 170 MHz. No FRBs were detected in the 2 s dedispersed images collected over 10.5 hr of observation covering 400 square degrees. This search placed a limit of <700 events/day/sky within the flux density limit of 700 Jy for a DM of 170–675 pc cm^{-3}. Rowlinson et al. (2016) conducted a survey for transient searches at 182 MHz with MWA using 28 s integration images. No FRBs were detected within the flux density limit of 0.285 Jy. The survey placed an upper limit of <82 FRBs/day/sky within the flux density limit of 7980 Jy for a DM < 700 pc cm^{-3}. Sokolowski et al. (2018) conducted coordinated MWA observations to shadow the low frequency component of the FRBs detected by the Australian Square Kilometre Array Pathfinder (ASKAP) at 1.4 GHz. The simultaneous MWA observations of seven ASKAP FRBs between 70 and 200 MHz using 0.5 s images did not detect any low frequency emission. The results from previous observations and smaller pulse width compared to the expected width from scattering implies that the observed transient is less likely to be an FRB event.

This also implies that the detected transient is new and at the same time it is similar to the transient detected by Stewart et al. (2016), ILT J225347+862146. The 6σ detection threshold of 38 MHz LASI images at zenith is 250 Jy (Obenberger et al. 2015a). The sensitivity of an 11 minute LOFAR MSSS image is greater than 7.9 Jy. The detected ILT J225347+862146 had a flux density of 20 Jy and an 11 minute duration. The LASI images are not sensitive enough to detect ILT J225347+862146. At the same time, LOFAR MSSS images could have easily detected LWAT 171018 as it was an 800 Jy bright event. But if ILT J225347+862146 lasted only for a 5 s duration, and assuming the fluence is same at 60 and 38 MHz, then the peak flux density of the event would be 2640 Jy. This event could be easily observed in LASI images. In the same way, if the 800 Jy LWAT 171018 lasted for 11 minutes in MSSS images, then the peak flux would be 19.09 Jy, which is also above the detection threshold.

6.3. Burst Location

An upper bound on the distance using the DM can be written as DM $\approx$ 1200 z pc cm^{-3} (Lorimer et al. 2007). So a DM of 804 pc cm^{-3} can give a redshift, $z \approx 0.67$. The observed contribution of DM from Milky Way is less than 100 pc cm^{-3} for Galactic latitudes greater than 10° (Yang & Zhang 2016). The total observed DM is the sum of the contribution from the host galaxy, intergalactic medium, and that of the Milky Way (Xu & Han 2015). After removing the contribution from the Milky Way a DM of 700 pc cm^{-3} gives redshift, $z \approx 0.58$. This is an upper limit of the redshift solely based on the temporal pulse width of the transient event.

7. Conclusions

By using two LWA stations separated by 75 km we present an anticoincidence study of the joint observations over a period of 10,240 hr between 2016 May and 2018 July. During this

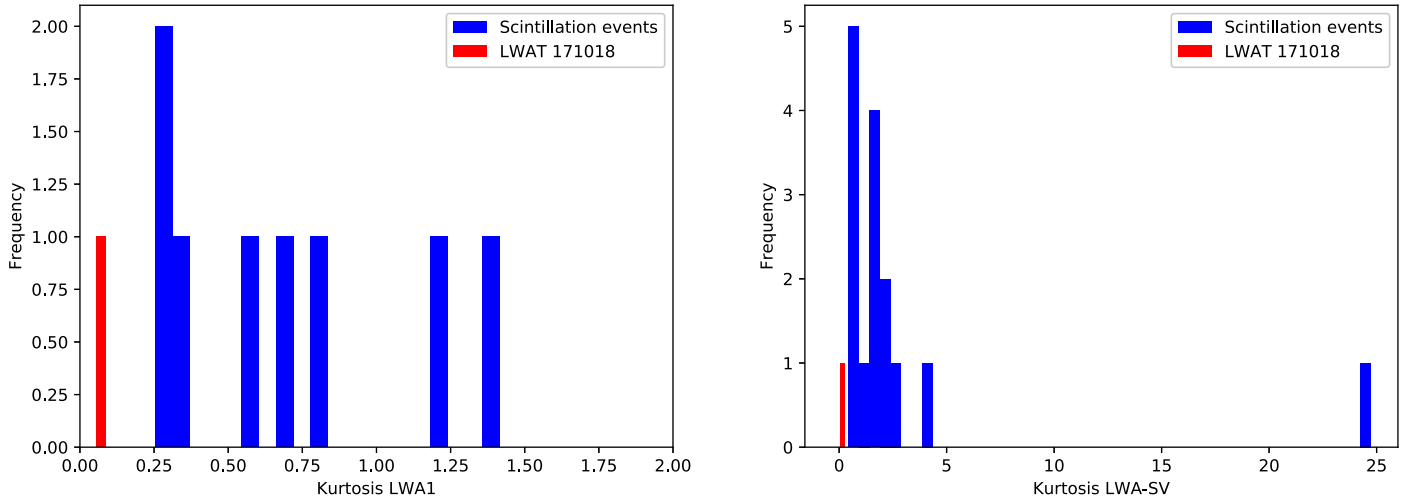

Figure 8. Histogram plot showing the kurtosis value of the scintillation from 4C +1.06 on different occasions in LWA (left) and LWA-SV (right) over the course of 10,240 hr of observation. The kurtosis value of the LWAT 171018 from each station are shown in red.

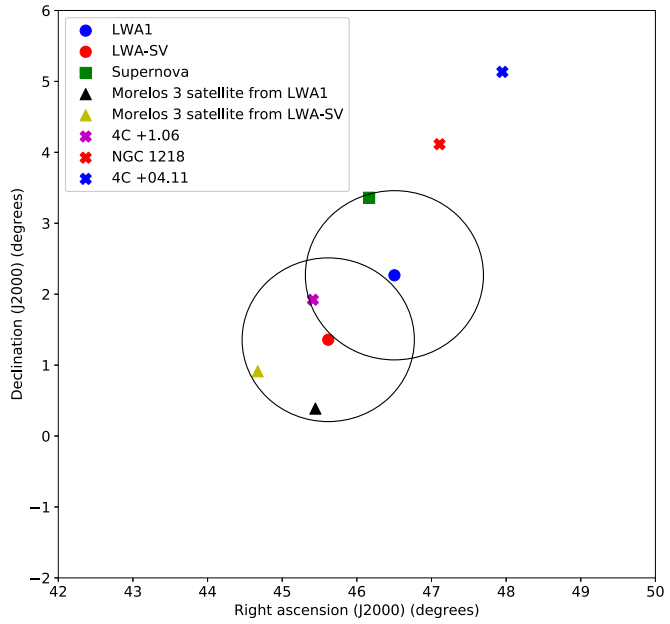

Figure 9. Plot showing the 1σ position error circle centered on the transient location from each station. The location of satellites seen from each station, optical supernova, and the VLSS sources 4C +1.06, NGC 1218, and 4C +04.11 is shown. The geometry is considered to be flat as the area shown is only $8^\circ \times 8^\circ$ in extent.

period 19 events were detected simultaneously from both stations in the same part of the sky; however, all but one of these can be classified as the result of scintillation of a known compact radio source induced by the ionosphere or RFI. One source on 2017 October 18 with a flux density of 840 Jy at 34 MHz is not readily explained by scintillation or RFI. After ruling out a number of possible origins we find that this new transient could be a previously unknown cosmic signal. The origin of this source is not clear due to the lack of evidence.

Multiepoch observations using sensitive telescopes at low frequencies may yield further emission signals if the transient source is still active. In the future, we will continue the all-sky monitoring to search for similar cosmic transient events using both LWA stations. Multiwavelength observations of cosmic transient sources followed by an LWA trigger could provide insights into the source structure and process of emission mechanisms. Future observations of similar transients will also benefit from the implementation of a broadband (10 MHz) all-sky correlator that now runs continuously at the LWA-SV station.

Construction of the LWA has been supported by the Office of Naval Research under Contract N00014-07-C-0147 and by the AFOSR. Support for operations and continuing development of the LWA1 is provided by the Air Force Research Laboratory and the National Science Foundation under grants AST-1711164 and AGS-1708855.

Facilities: LWA1, LWA-SV, Pan-STARRS.

Software: LWA Software Library (Dowell et al. 2012).

ORCID iDs

S. S. Varghese https://orcid.org/0000-0003-2669-0364
J. Dowell https://orcid.org/0000-0003-1407-0141
G. B. Taylor https://orcid.org/0000-0001-6495-7731

References

Bannister, K. W., Murphy, T., Gaensler, B. M., Hunstead, R. W., & Chatterjee, S. 2011, MNRAS, 412, 634
Bell, M. E., Murphy, T., Kaplan, D. L., et al. 2014, MNRAS, 438, 352
Carbone, D., van der Horst, A. J., Wijers, R. A. M. J., et al. 2016, MNRAS, 459, 3161
Coenen, T., van Leeuwen, J., Hessels, J. W. T., et al. 2014, A&A, 70, A60
Cohen, A. S., Lane, W. M., Cotton, W. D., et al. 2007, AJ, 134, 1245
Cordes, J. M., Lazio, T. J. W., & McLaughlin, M. A. 2004, NewAR, 48, 1459
Cranmer, M. D., Barsdell, B. R., Price, D.C., et al. 2017, JAI, 6, 1750007
Dowell, J., Wood, D., Stovall, K., et al. 2012, JAI, 01, 1250006
Eftekhari, T., Stovall, K., Dowell, J., et al. 2016, ApJ, 829, 62
Ellingson, S. W., Craig, J., Dowell, J., Taylor, G. B., & Helmboldt, J. F. 2013, arXiv:1307.0697
Farrell, W. M., Desch, M. D., & Zarka, P. 1999, JGR, 104, 14025
Guillochon, J., Parrent, J., Kelley, L.Z., & Margutti, R. 2017, ApJ, 835, 64G
Hallinan, G., Bourske, S., Lane, C., et al. 2007, ApJL, 663, L25
Hankins, T. H., Kern, J. S., Weatherall, J. C., & Eilek, J. A. 2003, Natur, 422, 141
Hassall, T. E., Keane, E. F., & Fender, R. P. 2013, MNRAS, 436, 371
Hyman, S. D., Lazio, T. J. W., Kassim, N. E., et al. 2005, Natur, 434, 50
Jackson, P. D., Kundu, M. R., & White, S. M. 1989, A&A, 210, 284
Jaeger, T. R., Hyman, S. D., Kassim, N. E., & Lazio, T. J. W. 2012, AJ, 143, 96
Xu, J., & Han, J. L. 2015, RAA, 15, 10

Karako-Argaman, C., Kaspi, V. M., Lynch, R. S., et al. 2015, ApJ, 809, 67
Karastergiou, A., Chennamangalam, J., Armour, W., et al. 2015, MNRAS, 452, 1254
Lane, W. M., Cotton, W. D., Helmboldt, J. F., & Kassim, N. E. 2012, RaSc, 47, 6
Lorimer, D. R., Bailes, M., McLaughlin, M. A., Narkevic, D. J., & Crawford, F. 2007, Sci, 318, 777
McLaughlin, M. A., & Cordes, J. M. 2003, ApJ, 596, 982
McLaughlin, M. A., Lyne, A. G., Lorimer, D. R., et al. 2006, Natur, 439, 817
Murphy, T., Kaplan, D.L., Croft, S., et al. 2017, MNRAS, 466, 1944
Obenberger, K. S., Hartman, J. M., Taylor, G. B., et al. 2014a, ApJ, 785, 270
Obenberger, K. S., Taylor, G. B., Hartman, J.M., et al. 2014b, ApJ, 788, 260
Obenberger, K. S., Taylor, G. B., Hartman, J.M., et al. 2015a, JAI, 04, 155004155004
Obenberger, K. S., Taylor, G. B., Lin, C. S., et al. 2015b, JGR, 120, 9916
Petroff, E., Barr, E. D., Jameson, A., et al. 2016, PASA, 33, e045
Rees, M. J. 1977, Natur, 266, 333
Roland, J. 1985, A&A, 148, 323
Rowlinson, A., Bell, M. E., Murphy, T., et al. 2016, MNRAS, 458, 3506
Sagiv, A., & Waxman, E. 2002, ApJ, 574, 861
Sokolowski, M., Bhat, N. D. R., Macquart, J. -P., et al. 2018, ApJL, 867, L12
Stewart, A. J., Fender, R. P., Broderick, J. W., et al. 2016, MNRAS, 456, 2321
Taylor, G. B., Ellingson, S. W., Kassim, N. E., et al. 2012, JAI, 1, 1
Taylor, G. B., Stovall, K., McCrackan, M., et al. 2016, ApJ, 831, 140
The CHIME/FRB Collaboration 2019a, Natur, 566, 230
The CHIME/FRB Collaboration 2019b, Natur, 566, 235
Thornton, D., Stappers, B., Bailes, M., et al. 2013, Sci, 341, 53
Tingay, S. J., Goeke, R., Bowman, J. D., et al. 2013, PASA, 30, 7
Tingay, S. J., Trott, C.M., Wayth, R. B., et al. 2015, ApJ, 150, 199
Trott, C. M., Tingay, S. J., & Wayth, R. B. 2013, ApJL, 776, L16
Usov, V. V., & Katz, J. I. 2000, A&A, 364, 655
van Haarlem, V. M. P., Wise, M. W., Gunst, A.W., et al. 2013, A&A, 556, A2
Wild, J. P., Smerd, S. F., & Weiss, A. A. 1963, ARA&A, 1, 291
Yang, Y., & Zhang, B. 2016, ApJL, 830, L31